Journal of Materials Chemistry A

Accepted Manuscript

ROYAL SOCIETY OF CHEMISTRY

www.rsc.org/materialsA

Journal Name

ARTICLE

A block copolymer enhances the efficiency of small-molecule bulk-heterojunction photovoltaics

Received 00th January 20xx,
Accepted 00th January 20xx

DOI: 10.1039/x0xx00000x

www.rsc.org/

Hsiu-Cheng Chen,[a] Yu-Wei Su,[a] and Kung-Hwa Wei[a]

Block copolymer can self-assemble into ordered structures having feature dimensions on the order of 10 to 100nm; we took advantage of the different polarities of the blocks of a low-molecular-wieght diblock copolymer polystyrene-*b*-poly(ethylene oxide) (PS-*b*-PEO) that interact differentially with small molecules and fullerenes to tune the extent of the phase separation in the solution-processed small-molecule bulk-heterojunction (SMBHJ) solar cells. We incorporated small amounts of a nanostructured PS-*b*-PEO to solar cells' active layers featuring 7,7′-{4,4-bis(2-ethylhexyl)-4*H*-silolo[3,2-*b*:4,5-*b*′]dithiophene-2,6-diyl}bis{6-fluoro-4-(5′-hexyl-[2,2′-bithiophen]-5-yl)benzo[*c*][1,2,5]thiadiazole} (p-DTS(FBTTh$_2$)$_2$) and [6,6]-phenyl-C$_{71}$-butyric acid methyl ester (PC$_{71}$BM) for optimizing morphology and thus enhancing devices' power conversion efficiency. For understanding the effect of PS-*b*-PEO on devices' performances, we used synchrotron grazing-incidence wide-angle X-ray scattering, atomic force microscopy and transmission electron microscopyto probe and to decipher the morphologies of the resulting SMBHJ thin films. Without undergoing any annealing process, a device with an active layer of p-DTS(FBTTh$_2$)$_2$:PC$_{71}$BM(1:1.5, w:w) that incorporated 0.5 wt % of PS-*b*-PEO and was processed with 1,8-diiodooctane solvent additive displayed a power conversion efficiency (PCE) of 7.3%, a relative increase of 2.5 times as compared to the PCE of 2.1% for the control device featuring only p-DTS(FBTTh$_2$)$_2$ and PC$_{71}$BM. Thus, incorporating this nanostructured block copolymer in the active layer allowed effective tuning of the small molecule active layer morphology and resulted in enhanced device efficiency.

Introduction

In recent years, some small-molecule bulk-heterojunction (SMBHJ) photovoltaics have demonstrated power conversion efficiencies (PCEs) closed to 10%.[1–3] This progress has resulted from elegant structural design of small molecules capable of broadly harvesting the solar spectrum while exhibiting high degrees of crystallinity, thereby greatly increasing device PCEs after blending with fullerenes in solvents and then processed through spin-coating. Various post-processing approaches—including thermal annealing,[4–7] solvent vapor annealing,[8,9] solvent surface treatment,[10,11] and the use of solvent additives[12–23]—have been adopted to obtain optimal morphologies for the active layers and, thereby, enhance the efficiencies of the BHJs. Highly efficient SMBHJ solar cells are particularly attractive[24-27] because their well-defined chemical structures minimize batch-to-batch variability in terms of molecular weight and thus have higher degrees of crystallinity,[28,29] as compared to that of conjugated polymers. In addition, small molecules are generally easier to purify than conjugated polymersare.[30]

Several highly efficient SMBHJ solar cells featuring 7,7′-{4,4-bis(2-ethylhexyl)-4*H*-silolo[3,2-*b*:4,5-*b*′] dithiophene-2,6-diyl}bis{6-fluoro-4-(5′-hexyl-[2,2′-bithiophen]-5-yl)benzo[*c*][1,2,5] thiadiazole} (p-DTS(FBTTh$_2$)$_2$ as the donor component and [6,6]-phenyl C$_{70}$ butyric acid methyl ester (PC$_{71}$BM) as the acceptor component have been reported recently.[31–34] In such studies, 1,8-diiodooctane (DIO)—a high-boiling-point processing solvent capable of decreasing the size of the fullerene domains and inducing the crystallization of polymer or small molecules—has typically been used as a processing additive to ensure the fabrication of highly efficient devices; in addition, DIO can induce finer and more evenly distributed domains in conjunction with continuous interpenetrating networks without any large-scale aggregation of either the donor or acceptor in the BHJ composition.[16] The addition of a small concentration (2.5 wt %) of high-molecular-weight (M_n = 20,000,000 g mol^{-1}) polystyrene can increase an active layer's

[a] Department of Materials Science and Engineering, National Chiao Tung University, 300 Hsinchu, Taiwan.

†Electronic Supplementary Information (ESI) available: Further details are given in Fig. S1-S5. See DOI: 10.1039/x0xx00000x

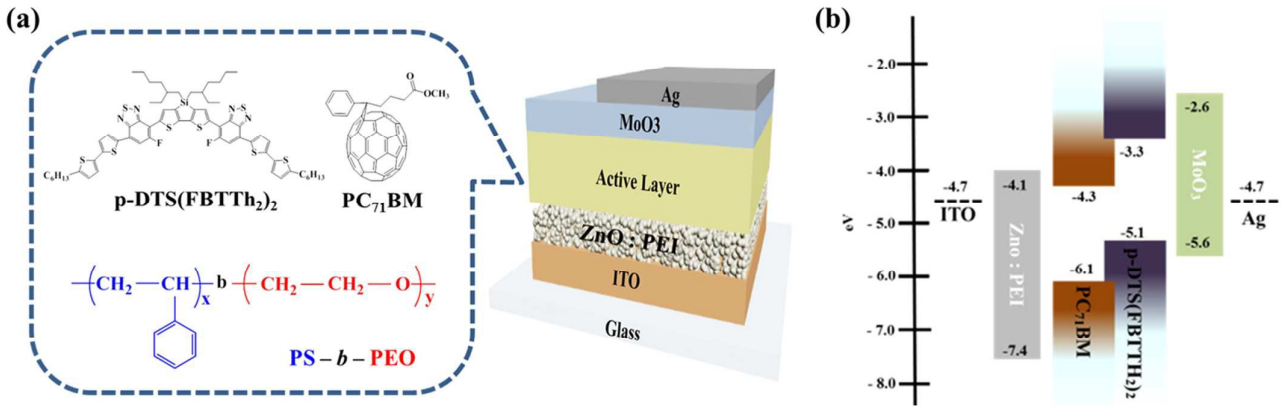

Fig. 1 (a) Inverted device structure of ITO/ZnO:PEI/SMBHJ/MoO_3/Ag. Inset shown molecular structures of p-DTS($FBTTh_2$)$_2$, $PC_{71}BM$, and PS-*b*-PEO ; (b) Energy level diagram of the component materials used in the inverted SMBHJ solar cells.

thickness without affecting its phase separation or structural order as reported previously.[35]

Block copolymers capable of self-assembling can form various nanostructured morphologies, including spherical micelles, worm micelles, lamellae, cylinders, and vesicles with dimensions on the order of 10 to 100nm.[36] Most previous studies have focused on the preparation of highly oriented and ordered arrays, the self-organization of block copolymers, and the potential applications of their phase transition behavior.[37–43] The major potential applications of such block copolymers are in the lithography of microelectronics, and electrical memory.[44–47] One particular block copolymer, polystyrene-*b*-poly(ethylene oxide) (PS-*b*-PEO), has been applied as a polymer blend compatibilizer, emulsifier, dispersant, stabilizer, and non-ionic surfactant.[48]

In this present study, we added a small amount (0.5wt%) of low-molecular-weight PS_{5k}-*b*-PEO_{5k}, comprising an amorphous PS block and a semi-crystalline PEO block, in the active layer based on p-DTS($FBTTh_2$)$_2$ and $PC_{71}BM$ as a means of tuning the extent of phase separation such as the small molecules lamellae size, fullerene cluster size and the extent of mixing between them, thereby achieving a high PCE. We term PS-*b*-PEO for PS_{5k}-*b*-PEO_{5k} in this paper thereafter. In addition, we employed a polyethyleneimine-doped sol–gel-processed zinc oxide/polyethyleneimine (ZnO:PEI) compositeas an electron transport layer in the inverted device structure.[49]

To the best of our knowledge, the incorporation of PS-*b*-PEO in the active layer of a SMBHJ solar cell has not been reported previously. We suspected that the large difference in polarity between the PEO (μ = 1.04 D) and PS (μ = 0.13 D) blocks would ensure their differential interactions with the small molecules (high dipole moment) and fullerenes (low dipole moment), respectively, thereby allowing effective tuning of the morphology of the active layer.[50,51] We employed X-ray scattering and electron microscopy techniques to examine the morphologies of the active layers in the SMBHJ solar cells, allowing us to discern the relationship between the active layer morphology and the device performance.

Table 1 Device parameters for solar cells containing p-DTS($FBTTh_2$)$_2$:$PC_{71}BM$ active layers spin-cast from CB solutions in the presence and absence of PS-*b*-PEO and DIO-processed. Ten devices were fabricated and measured for each condition.

p-DTS($FBTTh_2$)$_2$:$PC_{71}BM$	V_{oc} [V]	J_{sc} [mA cm^{-2}]	FF [%]	η [%]	μ_h [cm^2 V^{-1}s^{-1}]
Control	0.77± 0.01	9.52 ± 0.12	29.7± 0.5	2.1 ± 0.12	2.13x10^{-6}
PS-*b*-PEO (0.5 wt%)	0.77± 0.02	11.1± 0.09	30.8± 0.6	2.6 ± 0.13	5.07x10^{-6}
DIO-processed	0.78± 0.02	14.7± 0.14	46.3± 0.3	5.3 ± 0.11	1.45x10^{-5}
0.1wt%PS-*b*-PEO (DIO)	0.78± 0.01	16.3± 0.13	52.0± 0.3	6.6 ± 0.12	3.56x10^{-5}
0.5wt%PS-*b*-PEO (DIO)	0.78± 0.01	17.4± 0.11	54.4± 0.4	7.3 ± 0.11	4.28x10^{-5}
1.0wt%PS-*b*-PEO (DIO)	0.78± 0.01	16.8± 0.12	47.8± 0.3	6.3 ± 0.13	1.87x10^{-5}

V_{oc}: Open-circuit voltage; J_{sc}: short-circuit density; FF: fill factor ; η: power conversion efficiency; μ_h: hole mobility.

Results and discussion

Fig. 1(a) displays the molecular structures of p-DTS(FBTTH$_2$)$_2$, PC$_{71}$BM, and PS-*b*-PEO, as well as the device structure [indium tin oxide (ITO)/ZnO:PEI/p-DTS(FBTTH$_2$)$_2$:PC$_{71}$BM (1:1.5, w:w)/MoO$_3$/Ag]. All films were cast from chlorobenzene (CB), either with or without the solvent additive DIO. **Fig. 1 (b)** shows the energy levels diagram of component materials used in the device. The HOMOand LUMO energy levels of p-DTS(FBTTh$_2$)$_2$ are -5.1 and -3.3 eV,[31] and that of PC$_{71}$BM are -6.1 and -4.3 eV, respectively. **Fig. 2(a)** and **2(b)** display the current density–voltage (*J*–*V*) characteristics of inverted SMBHJ solar cells under 1 sun (simulated AM 1.5 G irradiation, 100 mW cm^{-2}) and their externalquantum efficiency (EQE) curves, respectively. **Table 1** summarizes the device characteristics of SMBHJ solar cells featuring active layersof p-DTS(FBTTH$_2$)$_2$:PC$_{71}$BM (1:1.5, w:w) in the presence of various amounts of PS-*b*-PEO. The control device featuring anactive layer of p-DTS(FBTTH$_2$)$_2$:PC$_{71}$BM (1:1.5, w:w) exhibited a short-circuit current (J_{sc}) of 9.5 mA cm^{-2}, an open circuit voltage (V_{oc}) of 0.77 V, a fill factor (FF) of 29.7%, and a PCE of 2.1%. When the active layer was processed using the solvent additive DIO at 0.4 vol %, the PCE of the device increased to 5.3%. On the other hand, when the active layer featured 0.5 wt % of PS-*b*-PEO within p-DTS(FBTTH$_2$)$_2$:PC$_{71}$BM (1:1.5, w:w) and was processed without DIO, the values of J_{sc} and FF increased slightly, resulting in the PCE of the device increasing to 2.6%—over 20% greater than that of the control device. After annealing at 80 °C for 10 min, the PCEs of the control, control-processed-with-DIO, and 0.5 wt % PS-*b*-PEO–containing devices improved to 3.4, 7.0, and 3.8%, respectively—from 2.1, 5.3, and 2.6%, respectively, in the absence of annealing (see Supplementary **Table S1** and **Fig. S1**). Thus, the improvement in PCE resulting from annealing of the devices improved substantially in the cases in the absence of PS-*b*-PEO, which is similar to the trend in the results of a previous study.[31] In the cases of without annealing, for the BHJ film incorporating 0.5wt% PS-*b*-PEO and having been processed with the additive DIO, the PCE of the device improved further to 7.3%—a relative increase of 2.5 times—as compared to that of the control case of 2.1%; it also indicates a relative increase of 37% as compared to that of the DIO-processed control case of 5.3%. Hence, the largest improvement in PCE was in the without annealing case where 0.5 wt% PS-*b*-PEO was incorporated in the active layer that had been processed with DIO—that is most likely because of the processing conditions providing more time for PS-*b*-PEO to interact with the small molecules and fullerenes and to form self-assembled structures.

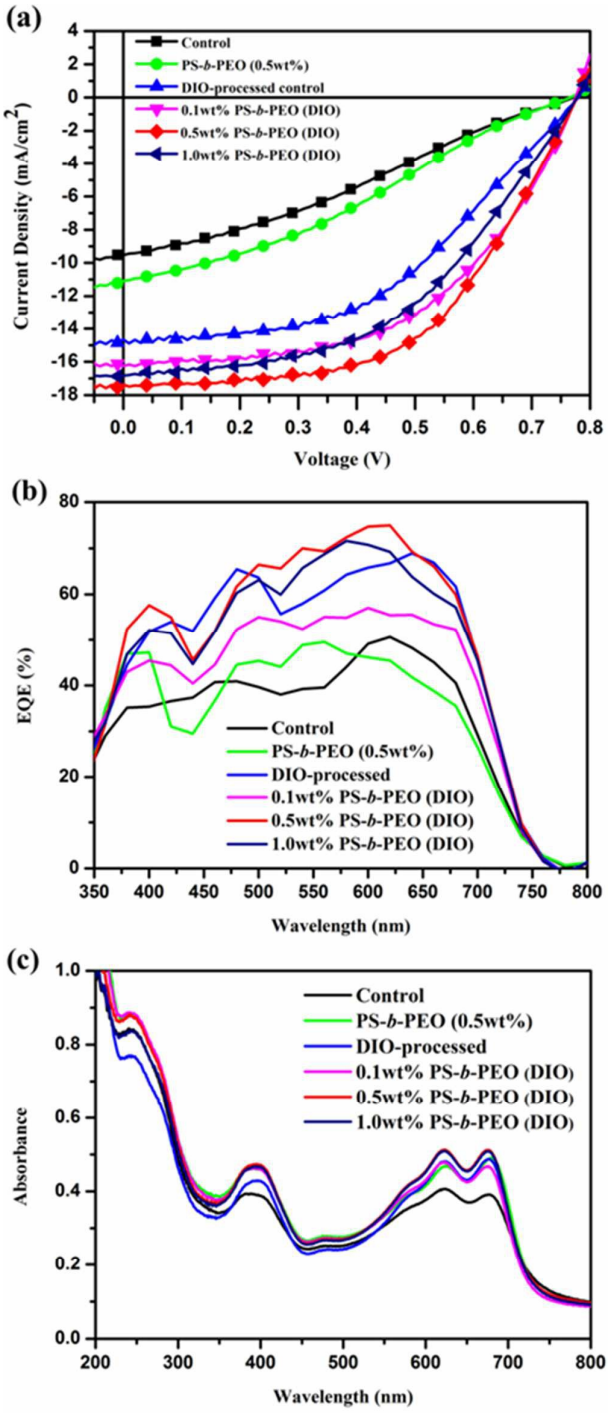

Fig. 2 (a) *J*–*V* characteristics; (b) EQE spectra; (c) UV–Vis absorption spectrum. The SMBHJ films were processed using p-DTS(FBTTh$_2$)$_2$:PC$_{71}$BM blended DIO or PS-*b*-PEO as additives.

The V_{oc} of all devices is about the same because the amount of PS-

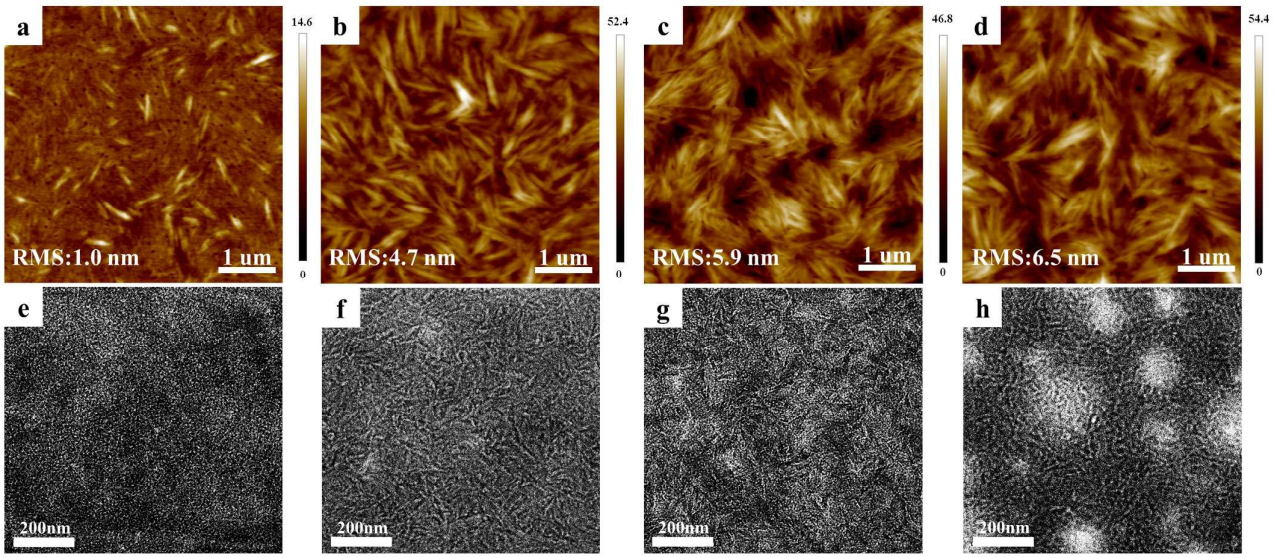

Fig. 3 (a–d) AFM topographic and (e–h) TEM images of p-DTS(FBTTh$_2$)$_2$:PC$_{71}$BM films; (a, e) Control; (b, f) DIO-processed; (c, g) 0.5 wt % PS-*b*-PEO with DIO-processed; (d, h) 1.0wt % PS-*b*-PEO with DIO-processed.

b-PEO present in the active layer is small (0.1 to 1wt%); this amount would affect the extent of phase separation to certain degree but not large enough to affect the V_{oc} that was mainly determined by the molecular parameters and affected by larger phase separation.

Fig. 2c presents UV–Vis absorption spectra of the spin-cast p-DTS(FBTTH$_2$)$_2$:PC$_{71}$BM (1:1.5, w:w) films (thickness: ca. 110 nm) that incorporated different amounts of PS-*b*-PEO. The spectra feature two broad vibronic peaks, at 625 and 675 nm, for the π–π stacked p-DTS(FBTTH$_2$)$_2$ aggregates, assigned to $A_{0\to1}$ and $A_{0\to0}$ transitions, respectively.[52,53] The p-DTS(FBTTH$_2$)$_2$:PC$_{71}$BM (1:1.5, w:w) films incorporating 0.5 wt % of PS-*b*-PEO and processed with 0.4 vol % of DIO displayed increases in absorbance for its peaks at 400, 625, and 675 nm.

To understand how the incorporated PS-*b*-PEO affected the p-DTS(FBTTH$_2$)$_2$:PC$_{71}$BM (1:1.5, w:w) active layer, we investigated the morphologies of thin films that have the same compositions as the ones used in solar cells using synchrotron grazing-incidence wide-angle X-ray scattering (GIWAXS), atomic force microscopy (AFM), and transmission electron microscopy (TEM). **Fig. 3(a–d)** display topological AFM images of the p-DTS(FBTTH$_2$)$_2$:PC$_{71}$BM (1:1.5, w:w) films. The film (**Fig. 3a**) for the control device had a very smooth surface, with root-mean-square (RMS) roughness of only 1.0 nm, with a minor fiber-like structure on this surface. The DIO-processed p-DTS(FBTTH$_2$)$_2$:PC$_{71}$BM (1:1.5, w:w) film (**Fig. 3b**) had a higher RMS roughness of 4.8 nm and show much more fiber-like p-DTS(FBTTH$_2$)$_2$ structure than that of the control film. The film of the p-DTS(FBTTH$_2$)$_2$:PC$_{71}$BM (1:1.5, w:w) that incorporates 0.5 wt % of PS-*b*-PEO presented (**Fig. S2a** in the supporting information) a disordered structure with p-DTS(FBTTH$_2$)$_2$ incorporated PEO-corolla and PS-coronaarising from the selectivity of the CB solvent; its RMS roughness was 4.4 nm. The DIO-processed p-DTS(FBTTH$_2$)$_2$:PC$_{71}$BM (1:1.5, w:w)/0.5 wt % PS-*b*-PEO film presented a fiber-like network structure with some phase separations (**Fig. 3c**). Whereas, The DIO-processed p-DTS(FBTTH$_2$)$_2$:PC$_{71}$BM (1:1.5, w:w)/1 wt % PS-*b*-PEO film show a more phase-separated system with smaller fiber-like structure (**Fig. 3d**). **Fig. 3(e–h)** present bright-field TEM images of the films prepared using conditions corresponding to those applied for AFM characterization. In **Fig. 3e**, the control film displays neither significant small-molecule p-DTS(FBTTH$_2$)$_2$ crystallization nor large phase separation between p-DTS(FBTTH$_2$)$_2$:PC$_{71}$BM (1:1.5, w:w) and PC$_{71}$BM. The DIO-processed film (**Fig. 3f**) displayed almost-distinct p-DTS(FBTTH$_2$)$_2$ fiber-like crystalline structure and slightly aggregated PC$_{71}$BM clusters. When 0.5wt% PS-*b*-PEO (**Fig. 3g**) was incorporated inp-DTS(FBTTH$_2$)$_2$:PC$_{71}$BM (1:1.5, w:w), relatively bright spot regions (diameter: 30 nm) appeared, attributed to the crystalline p-DTS(FBTTH$_2$)$_2$ fiber-incorporated PS-*b*-PEO domains, as well as dark regions, representing mixed phases of amorphous p-DTS(FBTTH$_2$)$_2$ intercalated into PC$_{71}$BM domains, reflecting the relatively high electron density of PC$_{71}$BM, indicating the extent of the phase separation of p-DTS(FBTTH$_2$)$_2$ and PC$_{71}$BM increased substantially. Compared with the 0.5 wt% PS-*b*-PEO incorporated

film, the p-DTS(FBTTH$_2$)$_2$ and PC$_{71}$BM(1:1.5, w:w) film incorporating 1.0wt % PS-*b*-PEO (**Fig. 3h**) that was processed with DIO had a morphology that featured a larger (40-60nm) white aggregation cluster region, suggesting that increasing the amount of incorporated PS-*b*-PEO led to the amorphous p-DTS(FBTTH$_2$)$_2$ incorporated PS-*b*-PEO aggregation cluster becoming larger and highly phase-separated characteristics in the film. For clarifying the thickness effect, we have checked our samples and found that the thickness variations for our TEM specimens are around 5 nm, and thus will not appreciably affect the contrast variations. Consequently, the contrast variation in **Fig. 3h** was mainly be attributed to the phase separation in the film. To investigate the cross-sectional morphologies and interfacial layer structures[49,54,55] that are important for the carrier transport in the inverted solar cell structure, we prepared a thin slice about 100nm of the device structure for TEM imaging with a focused ion beam technique. **Fig. S3** shows a high-resolution cross-sectional TEM image of the BHJ solar cell devices with a structure of ITO/ZnO:PEI/p-DTS(FBTTH$_2$)$_2$:PC$_{71}$BM:PS-*b*-PEO (0.5 wt%)/MoO$_3$/Ag by using the focused ion beam technique.

Typically, AFM and TEM reveal local information for BHJ films; GIWAXS and grazing-incidence small-angle X-ray scattering (GISAXS) are, on the other hand, complementary tools for probing multi-length-scale structures in BHJ films.[56,57] **Fig. 4a** presents the 2D GIWAXS pattern of the control (p-DTS(FBTTH$_2$)$_2$:PC$_{71}$BM)(1:1.5, w:w) film, demonstrating a highly disordered film that was responsible for the relatively low PCE for the device that adopted the film as the active layer.[14] The DIO-processed control film (**Fig. 4b**) exhibited relatively strong scattering patterns of its (001) peak as well as higher-order scattering peaks (002) and (003) along the q_z axis, indicating a lamella-like layered structure. When 0.5 wt % of PS-*b*-PEO was incorporated in the DIO-control film, the diffraction pattern (**Fig. 4c**) was similar to that of the DIO-processed control film prepared without PS-*b*-PEO, albeit with a slightly lower intensity. When the1.0wt% PS-*b*-PEO was incorporated in the active layer and was processed with DIO, the scattering pattern of the film (**Fig. 4d**) was almost identical to that of 0.5 wt % PS-*b*-PEO film. Previous reports have suggested that the crystallization of p-DTS(FBTTH$_2$)$_2$ in the BHJ can be enhanced significantly through either thermal annealing or processing with the additive DIO.[14,15,58] In our present study, the incorporation of PS-*b*-PEO into the p-DTS(FBTTH$_2$)$_2$:PC$_{71}$BM active layer enhanced the solar cell performance of the device without the need for additional thermal annealing.

The scattering pattern of the PS-*b*-PEO–incorporated, DIO-processed samples featured characteristic (001), (002), (003), and (010) peaks at 2.8, 5.6, 8.4, and 17.3 nm^{-1}, respectively (**Fig. S4** in the supporting information). These peaks matched well with those of single crystal refinement due to a lamella-like layered structure and DIO-processed thin film structure of p-DTS(FBTTH$_2$)$_2$ reported

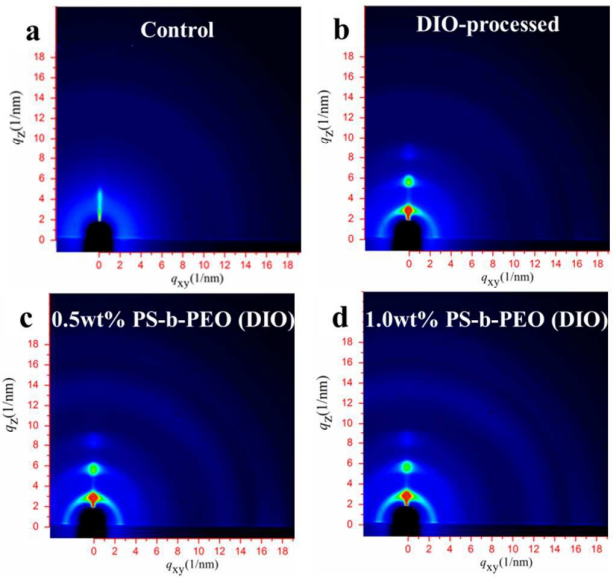

Fig.4 2D GIWAXS patterns of p-DTS(FBTTh$_2$)$_2$:PC$_{71}$BM films: (a) control; (b) DIO-processed film (c)0.5 wt % PS-*b*-PEO with DIO-processed; (d) 1.0wt % PS-*b*-PEO with DIO-processed. (The vertical lone profile q_{xy}≈ 0 is displayed in **Fig. S4**)

elsewhere.[14,15] We determined *d*-spacing using the equation (1)

$$d = 2\pi/q \quad (1)$$

We attribute the (001) peak at 2.8 nm^{-1} to alkyl chain stacking (d_{001} = 2.2 nm), while the broad peak at 13.2 nm^{-1} has several possible contributors: an amorphous region of p-DTS(FBTTH$_2$)$_2$ or PC$_{71}$BM, molecularly mixed domains of p-DTS(FBTTH$_2$)$_2$ and PC$_{71}$BM, and scattering from the substrate. The (010) peak along 17.3 nm^{-1} reflects π–π interchain stacking (d_{010} = 0.4 nm).[14,15,35,58,59] This finding is consistent with the lamella structure of p-DTS(FBTTH$_2$)$_2$ in the DIO-processed films. We also calculated the relative crystallinity of each case that was determined using the area under the (001) diffraction peak divided by all the peaks' area enclosed by curves

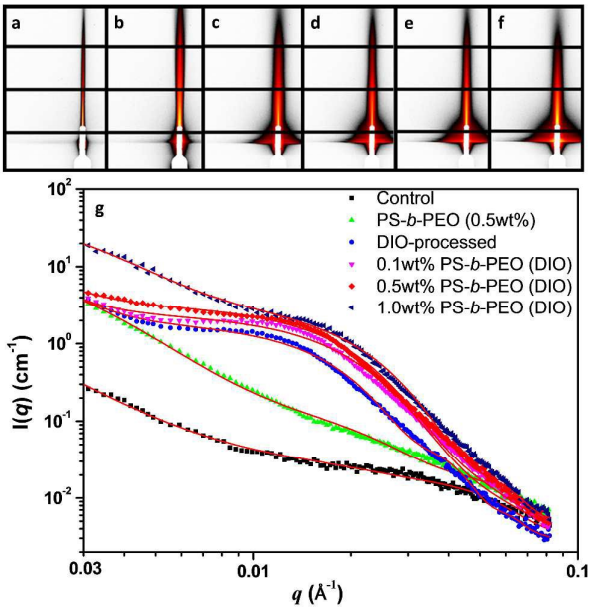

Fig. 5 2D GISAXS patterns of (a) control; (b) 0.5wt % PS-*b*-PEO; (c) DIO-processed; (d) 0.1wt % PS-*b*-PEO (DIO); (e) 0.5wt % PS-*b*-PEO (DIO); (f) 1.0wt % PS-*b*-PEO (DIO); (g) GISAXS profiles of p-DTS(FBTTh$_2$)$_2$:PC$_{71}$BM containing various weight fractions of PS-*b*-PEO, processed with and without the additive DIO. All of the profiles were fitted with calculated model intensities (solid lines).

approximation for hard-sphere interactions; V is the average cluster volume; and Δρ is the scattering length density contrast between the PC$_{71}$BM cluster and the matrix. The fitting parameters η, R, and p are the volume fraction, mean radius, and poly-dispersity of the size distribution of the PC$_{71}$BM clusters, respectively. The $f(\sigma)$ is Schulz size distribution. The detail SAXS fitting model is described in previous reference.[57] **Table 2** gives the whole sets of sizes for the p-DTS(FBTTH$_2$)$_2$ and PC$_{71}$BM in these BHJ films.

Considering the characteristics of these BHJ films (**Table 2**) and the device parameters (**Table 1**) altogether, the incorporation of a small amount, 0.5 wt%, of PS-*b*-PEO into the control film can induce

Table 2 Characteristics of fiber size and relative crystallinity of p-DTS(FBTTh$_2$)$_2$ and PC$_{71}$BM cluster radius in bulk-heterojunction films.

p-DTS(FBTTh$_2$)$_2$:PC$_{71}$BM	Fiber size Width/ Length[a] [nm]	Crystallinity [%]	PC$_{71}$BM Cluster radius[b] [nm]
Control	N/A	33%	4
DIO-processed	12/66	54%	6
0.5wt%PS-*b*-PEO (DIO)	11/69	51%	9
1.0wt%PS-b-PEO (DIO)	10/91	51%	8

[a]Determine from the TEM images; [b]PCBM cluster radius was calculated using a fractal poly-disperse aggregation model.

(see **Fig. S4** in the supporting information)

Fig. 5 show the line cut profiles for the DIO-processed films along the in-plane direction, q_x, of the 2D GISAXS images present broad humps in the medium-q region (0.006–0.06 Å^{-1}). Such broad humps can be attributed to the aggregation of PC$_{71}$BM into nanoscale clusters.[60] We used a poly-disperse sphere model having Schulz size distribution with hard-sphere interactions between PC$_{71}$BM clusters to model I(Q)$_{PCBM}$ peak for obtaining of the PC$_{71}$BM clusters, indicated by equation (2):

$$I_{PCBM}(Q) = \eta V(\Delta\rho)^2[\int_0^\infty F_i(Q,\sigma_i)^2 f(\sigma_i)\,d\sigma_i + \int_0^\infty\int_0^\infty F_i(Q,\sigma_i)F_j(Q,\sigma_j)H_{ij}(Q,\sigma_i,\sigma_j) f_i(\sigma_i)f_j(\sigma_j)\,d\sigma_i\,d\sigma_j] \quad (2)$$

where $F(Q, \sigma_i)^2$ is the form factor of a spherical PC$_{71}$BM cluster having a diameter σ_i; $H(Q, \sigma_i, \sigma_j)$ is the pair structure function describing the interaction between clusters with a Percus−Yevick

a slightly larger phase-separation of p-DTS(FBTTH$_2$)$_2$ with the PC$_{71}$BM as indicated by the PC$_{71}$BM cluster size increases to 9 nm from 6nm for the case of the DIO-processed control film, an increase of 50%. While the p-DTS(FBTTH$_2$)$_2$ fiber size becomes a little bit finer than that in the case of DIO-processed control film, but the crystallinity of p-DTS(FBTTH$_2$)$_2$ in both cases are about the same. As a result, the device's short current density and fill factor for the 0.5 wt% PS-*b*-PEO–incorporated and DIO-processed device increases to 17.4 mA/cm^2 and 54.4%, respectively, from 14.7 mA/cm^2 and 46.3% for the DIO-processed control device without any PS-*b*-PEO, leading to a significant relative increase of 37% in PCE (from 5.3 to 7.3%). This increase in the short current density and fill factor of the 0.5 wt% PS-*b*-PEO–incorporated and DIO-processed device can be attributed to the fact that the more intensive phase separation in the active layer that comprises larger fullerene cluster and aggregated small molecule crystals can provide optimum intertwined pathways for holes and electrons transport, as indicated by the large increase in the hole mobility for

the 0.5 wt% PS-*b*-PEO–incorporated case over that in the DIO-processed case, which is consistent with the results of a previous study.[61] In the case of 1.0 wt% PS-*b*-PEO–incorporated and DIO-processed device, since the relative crystallinity of p-DTS($FBTTH_2$)$_2$ and $PC_{71}BM$ cluster size are about the same but the phase separation becomes severe, the short current density is thus reduced, as also indicated by the low hole mobility (see **Table 1 and Fig. S5** in the supporting information). In **Table 1**, since with fullerene in the active layer the electron mobility is usually higher than hole mobility as reported by a previous study,[62] increasing hole mobility will enhance balanced charge transport in the devices and thus results in higher Jsc and device efficiency.

Conclusions

A block copolymer, PS-*b*-PEO, can self-assemble into ordered structures having feature dimensions on the order of 10–100nm. We have taken advantage of the different polarities of the PEO and PS blocks of PS-*b*-PEO di-block copolymer that interact differentially with p-DTS($FBTTh_2$)$_2$ and $PC_{71}BM$, respectively, to tune the extent of the phase separation of the SMBHJ active layer by varying its amount—leading to optimized structure and enhanced device efficiency. Based on the AFM, TEM and GIWAXS/GISAXS results, the incorporation of a small amount, 0.5 wt%, of PS-*b*-PEO into the control active layer and processed with DIO can induce a slightly larger phase-separation of p-DTS($FBTTH_2$)$_2$ with a large increase in the $PC_{71}BM$ cluster size and slightly more phase-separated p-DTS($FBTTH_2$)$_2$. A control device featuring p-DTS($FBTTH_2$)$_2$:$PC_{71}BM$ as the active layer achieved a PCE of 2.1% and 5.3% without and with DIO additive processing, respectively. Incorporating 0.5wt% of PS-*b*-PEO in the p-DTS($FBTTH_2$)$_2$:$PC_{71}BM$ active layer and processing with DIO solvent additive, we achieved a device PCE of 7.3% without the need to perform any annealing processes. When compared with the PCEs of the control and DIO-processed devices, the PCE of the device incorporating the DIO-processed, 0.5wt% PS-*b*-PEO–containing BHJ active layer was enhanced by 3.5- and 1.4-fold, respectively. Thus, incorporating this nanostructured block copolymer in the active layer allowed effective tuning of the active layer morphology and resulted in enhanced device efficiency.

Experimental

Materials

The asymmetric PS-*b*-PEO diblock copolymer (Polymer Source) had molecular weights of PS and PEO blocks of 5000 and 5000 g mol^{-1}, respectively. The p-DTS($FBTTh_2$)$_2$ and $PC_{71}BM$ were purchased from 1-Material and Solenne BV, respectively. All these materials were used without further purification. ZnO:PEI sol-gel was prepared by first dissolving zinc acetate dihydrate [$Zn(CH_3COO)_2{\cdot}2H_2O$ (1.0 g)] in ethanolamine (0.28 g) and branched PEI in 2-methoxyethanol (10 mL), and then the two solutions being mixed together under vigorous stirring for 12 h. The detailed procedure has been reported previously.[49] A p-DTS($FBTTh_2$)$_2$:$PC_{71}BM$ (donor/acceptor) blend solution was prepared at a weight ratio of 3:2; it incorporated 0.1, 0.5, or 1.0 wt % of PS-*b*-PEO and 0.4 vol % of DIO in CB at an overall concentration of 35 mg mL^{-1}.

Device fabrication

The ITO-coated glass substrates were cleaned sequentially by detergent, deionized water, acetone, and isopropyl alcohol with ultrasonication, and then exposed to UV/ozone treatment for 15 min to reform the surface. The prepared ZnO:PEI sol–gel was spin-cast on the ITO-coated glass substrate (4000 rpm, 40 s). The film was annealed in air at 200 °C for 1 h. The thickness of the ZnO:PEI film was approximately 40 nm. The small molecule/fullerene blend solution was stirred overnight at 80 °C and heated at 90 °C for 15 min before spin-casting. The SMBHJ film was obtained through spin-casting (1500 rpm, 45 s) and then drying for 30 min. The final film thickness was approximately 110 nm. Device fabrication was complete after thermal evaporation of the P-type material (MoO_3,10 nm) and the anode (Ag, 100 nm) under high vacuum (ca. 10^{-7}torr). A shadow mask was used during the thermal evaporation process to define a device area of 0.1 cm^2.

Device characterization

The *J*–*V* characteristics were measured using a Keithley 2400 source meter. The photocurrent was measured under simulated AM 1.5 G illumination at 100 mW cm^{-2} using a Xe lamp–based 150-W solar simulator (Newport 66902). A calibrated Si photodiode with a KG-5 filter was employed to confirm the illumination intensity. The spectral mismatch factor was calculated by comparing the solar simulator spectrum with the AM1.5G (ASTM G173) spectrum. We carried out the I-V measurement of the devices without using a light mask for setting the device area, and thus the edge of the devices might affect the device measurement results to some extent. We, however, compared the results on the same basis, and hence the

trend is reliable. EQEs were measured using an SRF50 system (Optosolar, Germany). A calibrated mono-silicon diode was used as a reference exhibiting a response at 300–800 nm. The thickness of the active layer in the device was measured using a Veeco Dektak 150 surface profiler. Sample films were prepared by spin-casting p-DTS(FBTTh$_2$)$_2$:PC$_{71}$BM solutions onto either 4-cm^2 quartz (for UV–Vis spectroscopy) or a silicon wafer [for AFM, and GIWAXS]. For preparation of TEM specimens, p-DTS(FBTTh$_2$)$_2$:PC$_{71}$BM solutions were spin-cast onto ITO glass, which had a PEDOT:PSS layer on its surface. The films floated off the substrate after immersing the samples in deionized water; the floating fragment was collected on a TEM grid and dried under vacuum. We have tried to prepare TEM specimens by floating them from ZnO:PEI layer, but it is difficult to obtain the intact p-DTS(FBTTh$_2$)$_2$:PC$_{71}$BM films on the copper grid, and thus we chose PEDOT:PSS as the substrate for the TEM sample preparations. The substrate can play a significant role in affecting morphology of the film that was deposited on its top, but its influence declined with the increasing film thickness. We prepared films with thickness about 95nm, and thus there are some substrate effects. On the other hand, we also compared the morphology results on the relative basis, and hence the effects on the relative differences in the morphology of the films can be minimized. A spectrophotometer (Hitachi U-4100) equipped with an integrating sphere was used to acquire UV–Vis absorbance spectra. Film morphologies were determined through AFM (Veeco Innova) performed in the tapping mode. TEM (JEOL-2010**)** images were recorded at a beam energy of 200 keV. GIWAXS analysis [X-ray beam energy: 10 keV (λ = 1.24 Å); incident angle: 0.15°] was conducted in BL23A SWAXS of the National Synchrotron Radiation Research Center (NSRRC), Hsinchu, Taiwan.

SCLC mobility measurement

The hole-only diodes structures were similar to that of the solar cell devices; we fabricated the hole-only devices with the structures of ITO/PEDOT:PSS/SM BHJ with PS-*b*-PEO/MoO_3(10nm)/Ag(100nm). Dark J-V characteristics of the hole-only devices were measured and using the space-charge limited current (SCLC) model, as described by the Mott-Gurney law, $\mathbf{J} = \frac{9}{8}\boldsymbol{\varepsilon_0}\boldsymbol{\varepsilon_r}\boldsymbol{\mu}\frac{\mathbf{V^2}}{\mathbf{L^3}}$, where J is the current density, $\varepsilon_0\varepsilon_r$ is the dielectric permittivity of the active layer (p-DTS(FBTTh$_2$)$_2$:PC$_{71}$BM blend with PS-*b*-PEO); L is the thickness of the active layer; μ is the zero-field mobility; V is the internal voltage in the device, and $V = V_{appl} - V_{bi} - V_{rs}$, where V_{appl} is the applied voltage, V_{bi} is the built-in voltage which resulting from the relative work function difference between the two electrodes, and V_{rs} is the voltage drop resulting from the relative work function difference.

Acknowledgements

We thank the National Science Council, Taiwan, for financial support (MOST 103-2221-E-009-211-MY3).

Notes and references

1 Q. Zhang, B. Kan, F. Liu, G. Long, X. Wan, X. Chen, Y. Zuo, W. Ni, H. Zhang, M. Li, Z. Hu, F. Huang, Y. Cao, Z. Liang, M. Zhang, T. P. Russell and Y. Chen, *Nat Photon*, 2015, **9**, 35.

2 B. Kan, Q. Zhang, M. Li, X. Wan, W. Ni, G. Long, Y. Wang, X. Yang, H. Feng and Y. Chen, *J. Am. Chem. Soc.*, 2014, **136**, 15529.

3 Y. Liu, C.-C. Chen, Z. Hong, J. Gao, Y. Yang, H. Zhou, L. Dou and G. Li, *Sci. Rep.*, 2013, **3**, 3356.

4 W. Ma, C. Yang, X. Gong, K. Lee and A. J. Heeger, *Adv. Funct. Mater.*, 2005, **15**, 1617.

5 Y. Kim, S. Cook, S. M. Tuladhar, S. A. Choulis, J. Nelson, J. R. Durrant, D. D. C. Bradley, M. Giles, I. McCulloch, C.-S. Ha and M. Ree, *Nat. Mater.*, 2006, **5**, 197.

6 G. Li, V. Shrotriya, J. Huang, Y. Yao, T. Moriarty, K. Emery and Y. Yang, *Nat. Mater.*, 2005, **4**, 864.

7 X. Yang, J. Loos, S. C. Veenstra, W. J. H. Verhees, M. M. Wienk, J. M. Kroon, M. A. J. Michels and R. A. J. Janssen, *Nano Lett.*, 2005, **5**, 579.

8 G. Li, Y. Yao, H. Yang, V. Shrotriya, G. Yang and Y. Yang, *Adv. Funct. Mater.*, 2007, **17**, 1636.

9 K. Sun, Z. Xiao, E. Hanssen, M. F. G. Klein, H. H. Dam, M. Pfaff, D. Gerthsen, W. W. H. Wong and D. J. Jones, *J. Mater. Chem. A*, 2014, **2**, 9048.

10 M. A. Ruderer, S. Guo, R. Meier, H.-Y. Chiang, V. Körstgens, J. Wiedersich, J. Perlich, S. V. Roth and P. Müller-Buschbaum, *Adv. Funct. Mater.*, 2011, **21**, 3382.

11 L. Ye, Y. Jing, X. Guo, H. Sun, S. Zhang, M. Zhang, L. Huo and J. Hou, *J. Phys. Chem. C*, 2013, 117, 14920.

12 J. W. Rumer, R. S. Ashraf, N. D. Eisenmenger, Z. Huang, I. Meager, C. B. Nielsen, B. C. Schroeder, M. L. Chabinyc and I. McCulloch, *Adv. Energy Mater.*, 2015, **5**, 1401426.

13 M.-S. Su, C.-Y. Kuo, M.-C. Yuan, U. S. Jeng, C.-J. Su and K.-H. Wei, *Adv. Mater.*, 2011, **23**, 3315.

14 J. A. Love, C. M. Proctor, J. Liu, C. J. Takacs, A. Sharenko, T. S. van der Poll, A. J. Heeger, G. C. Bazan and T.-Q. Nguyen, *Adv. Funct. Mater.*, 2013, **23**, 5019.

15 L. A. Perez, K. W. Chou, J. A. Love, T. S. van der Poll, D.-M. Smilgies, T.-Q. Nguyen, E. J. Kramer, A. Amassian and G. C. Bazan, *Adv. Mater.*, 2013, **25**, 6380.

16 J. D. A. Lin, O. V. Mikhnenko, T. S. van der Poll, G. C. Bazan and T.-Q. Nguyen, *Adv. Mater.*, 2015, **27**, 2528.

17 A. K. K. Kyaw, D. H. Wang, V. Gupta, J. Zhang, S. Chand, G. C. Bazan and A. J. Heeger, *Adv. Mater.*, 2013, **25**, 2397.

18 A. K. K. Kyaw, D. H. Wang, V. Gupta, W. L. Leong, L. Ke, G. C. Bazan and A. J. Heeger, *ACS Nano*,2013, **7**, 4569.
19 C. McDowell, M. Abdelsamie, K. Zhao, D.-M. Smilgies, G. C. Bazan and A. Amassian, *Adv. Energy Mater*., 2015, **5**, 1501121.
20 H.-C. Liao, C.-C. Ho, C.-Y. Chang, M.-H. Jao, S. B. Darling and W.-F. Su, *Materials Today*, 2013, **16**, 326.
21 W. Chen, M. P. Nikiforov and S. B. Darling, *Energy Environ. Sci*., 2012, **5**, 8045.
22 C.-M. Liu, Y.-W. Su, J.-M. Jiang, H.-C. Chen, S.-W. Lin, C.-J. Su, U. S. Jeng and K.-H. Wei, *J. Mater.Chem. A*, 2014, **2**, 20760-20769.
23 Y.-W. Su, S.-C. Lan and K.-H. Wei, *Materials Today*, 2012, **15**, 554-562.
24 Y. Sun, G. C. Welch, W. L. Leong, C. J. Takacs, G. C. Bazan and A. J. Heeger, *Nat. Mater.*, 2012, **11**, 44.
25 M. L. Petrus, F. S. F. Morgenstern, A. Sadhanala, R. H. Friend, N. C. Greenham and T. J. Dingemans, *Chem. Mater*., 2015, **27**, 2990.
26 Y. Chen, X. Wan, G. Long, *Acc. Chem. Res*., 2013, **46**, 2645.
27 O. P. Lee, A. T. Yiu, P. M. Beaujuge, C. H. Woo, T. W. Holcombe, J. E. Millstone, J. D. Douglas, M. S. Chen and J. M. J. Fréchet, *Adv. Mater*., 2011, **23,** 5359.
28 B. Walker, C. Kimand T.-Q. Nguyen, *Chem. Mater*., 2011, **23**, 470.
29M. E. Farahat, H.-Y. Wei, M. A. Ibrahem, K. M. Boopathi, K.-H. Wei and C.-W. Chu, RSC Advances, 2014, 4, 9401-9411.
30M. P. Nikiforov, B. Lai, W. Chen, S. Chen, R. D. Schaller, J. Strzalka, J. Maser and S. B. Darling, *Energy Environ.Sci*., 2013, 6, 1513.
31 T. S. van der Poll, J. A. Love, T.-Q.Nguyen and G. C. Bazan, *Adv. Mater*., 2012, **24**, 3646.
32 B. C. Schroeder, Z. Huang, R. S. Ashraf, J. Smith, P. D'Angelo, S. E. Watkins, T. D. Anthopoulos, J. R. Durrant and I. McCulloch, *Adv. Funct. Mater*., 2012, **22**, 1663.
33 S. Mukherjee, C. M. Proctor, G. C. Bazan, T.-Q. Nguyen and H. Ade, *Adv. Energy Mater*.,2015, **5**, 1500877.
34 D. H. Wang, J. K. Kim, S. Jin Kim, B. Hee Hong and J. H. Park, *Nanoscale*, 2014, **6**, 15175.
35 Y. Huang, W. Wen, S. Mukherjee, H. Ade, E. J. Kramer and G. C. Bazan, *Adv. Mater*., 2014, **26**, 4168.
36 R. J. Williams, A. P. Doveand R. K. O'Reilly, *Polym. Chem*., 2015, **6**, 2998.
37 S.-W. Yeh, K.-H. Wei, Y.-S. Sun, U. S. Jeng and K. S. Liang, *Macromolecules*, 2003, **36**, 7903.
38 A. E. Di Mauro, M. Striccoli, N. Depalo, E. Fanizza, L. Cano, C. Ingrosso, A. Agostiano, M. L. Curri and A. Tercjak, *Soft Matter*, 2014, **10**, 1676.
39 S. H. Kim, M. J. Misner, T. Xu, M. Kimura and T. P. Russell, *Adv. Mater*., 2004, **16**, 226.
40 B. Kim, S. W. Hong, S. Park, J. Xu, S.-K. Hong and T. P. Russell, *Soft Matter*, 2011, **7**, 443.
41 Y. Zhao, K. Thorkelsson, A. J. Mastroianni, T. Schilling, J. M. Luther, B. J. Rancatore, K. Matsunaga, H. Jinnai, Y. Wu, D. Poulsen, J. M. J. Frechet, A. Paul Alivisatos and T. Xu, *Nat. Mater*., 2009, **8**, 979.
42 D. Kipp, J. Mok, J. Strzalka, S. B. Darling, V. Ganesan and R. Verduzco, *ACS Macro Letters*, 2015, **4**, 867.
43 J. A. Amonoo, A. Li, G. E. Purdum, M. E. Sykes, B. Huang, E. F. Palermo, A. J. McNeil, M. Shtein, Y.-L. Loo and P. F. Green, *J. Mater. Chem. A*, 2015, **3**, 20174.
44 C. M. Bates, M. J. Maher, D. W. Janes, C. J. Ellison and C. G. Willson, *Macromolecules*, 2014, **47**, 2.
45 C.-M. Chen, C.-M. Liu, M.-C. Tsai, H.-C. Chen and K.-H. Wei, *J. Mater. Chem. C*, 2013, **1**, 2328.
46 S. B. Darling, *Energy Environ*. Sci., 2009, **2**, 1266.
47 Y. S. Jung, J. B. Chang, E. Verploegen, K. K. Berggren and C. A. Ross, *Nano Lett*., 2010, **10**, 1000.
48 T. Ghoshal, T. Maity, R. Senthamaraikannan, M. T. Shaw, P. Carolan, J. D. Holmes, S. Roy and M. A. Morris, *Sci. Rep*., 2013, **3**,2772.
49 H.-C. Chen, S.-W. Lin, J.-M. Jiang, Y.-W. Su and K.-H. Wei, *ACS Appl. Mater. Interfaces*, 2015, **7**, 6273.
50 N. Yamaguchi, M. Sato, *Polym. J*., 2009, **41**, 588.
51 H. Stange and A. Greiner, *Macromol. Rapid Commun*., 2007, **28**, 504.
52 F. C. Spano, *Acc. Chem. Res.*, 2010, **43**, 429.
53 N. Herath, S. Das, J. K. Keum, J. Zhu, R. Kumar, I. N. Ivanov, B. G. Sumpter, J. F. Browning, K. Xiao, G. Gu, P. Joshi, S. Smith and V. Lauter, *Sci. Rep*., 2015, **5**, 13407.
54 B. Murali, A. E. Labban, J. Eid, E. Alarousu, D. Shi, Q. Zhang, X. Zhang, O. M. Bakr and O. F. Mohammed, *Small*, 2015, **11**, 5272.
55 A. Bera, K. Wu, A. Sheikh, E. Alarousu, O. F. Mohammed and T. Wu, *J. Phys. Chem. C*, 2014, **118**, 28494.
56 C.-Y. Chen, C.-S.Tsao, Y.-C. Huang, H.-W. Liu, W.-Y. Chiu, C.-M. Chuang, U. S. Jeng, C.-J. Su, W.-R. Wu, W.-F. Su and L. Wang, *Nanoscale*, 2013, **5**, 7629.
57 Y.-C. Huang, C.-S. Tsao, T.-Y. Huang, H.-C. Cha, D. Patra, C.-J.Su, U. S. Jeng, K.-C. Ho, K.-H. Wei and C.-W. Chu, *J. Phy. Chem. C*, 2015, **119**, 16507.
58 S. Engmann, F. A. Bokel, A. A. Herzing, H. W. Ro, C. Girotto, B. Caputo, C. V. Hoven, E. Schaible, A. Hexemer, D. M. DeLongchamp and L. J. Richter, *J. Mater. Chem. A*, 2015, **3**, 8764.
59 A. Sharenko, N. D. Treat, J. A. Love, M. F. Toney, N. Stingelin and T.-Q. Nguyen, *J. Mater. Chem. A*, 2014, **2**, 15717.
60 W.-R. Wu, U. S. Jeng, C.-J. Su, K.-H. Wei, M.-S. Su, M.-Y. Chiu, C.-Y. Chen, W.-B. Su, C.-H. Su and A.-C. Su, *ACS Nano*, 2011, **5**, 6233.
61 M.-Y. Chiu, U-S. Jeng, K. S. Liang, C.-H. Su and K.-H. Wei, *Adv. Mater*.,2008, **20**, 2573.
62 M.-Y. Chiu, U. S. Jeng, M.-S. Su and K.-H. Wei, *Macromolecules*, 2010, **43**, 428.

Table of Contents

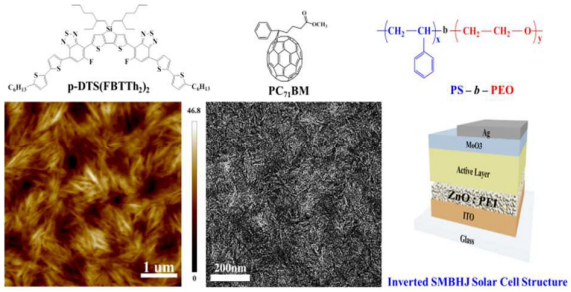

Using PS-*b*-PEO block copolymer in the active layer allowed effective tuning of the small molecule active layer morphology and enhanced device efficiency.